Journal of Solid State Chemistry 182 (2009) 2640–2645

Contents lists available at ScienceDirect

Journal of Solid State Chemistry

journal homepage: www.elsevier.com/locate/jssc

Two organic–inorganic poly(pseudo-rotaxane)-like composite solids constructed from polyoxovanadates and silver organonitrogen polymers

Yanfei Qi [a,b], Enbo Wang [b,*], Juan Li [a,*], Yangguang Li [b]

[a] School of Public Health, Jilin University, Changchun, Jilin 130021, PR China
[b] Key Laboratory of Polyoxometalates Science of Ministry of Education, Department of Chemistry, Northeast Normal University, Changchun, Jilin 130024, PR China

ARTICLE INFO

Article history:
Received 16 January 2009
Received in revised form
24 June 2009
Accepted 12 July 2009
Available online 22 July 2009

Keywords:
Polyoxovanadates
Silver–organonitrogen complexes
Entangled networks
Organic–inorganic hybrid
Electrochemical property

ABSTRACT

Two new composite solids, $[Ag(btx)]_4H_2V_{10}O_{28}\cdot 2H_2O$ **1** and $[Ag(biim)]_2V_4O_{11}$ **2** (btx = 1,4-bis(triazol-1-ylmethyl)benzene, biim = 1,1′-(1,4-butanediyl)bis(imidazole)), have been synthesized and characterized by elemental analysis, IR, TGA and single-crystal X-ray diffraction. Compound **1** contains two one-dimensional (1D) polymeric chains, $\{Ag_2(btx)_2\}^{2+}$ and $[Ag_2(btx)_2H_2V_{10}O_{28}]^{2-}$, that are assembled by supramolecular forces into an intriguing two-dimensional (2D) poly(pseudo-rotaxane) network. Compound **2** comprises cationic $\{Ag_2(biim)_2\}^{2+}$ three-dimensional (3D) framework penetrated by anionic $[V_4O_{11}]_n^{2n-}$ chains. The electrochemical properties of the two compounds have been studied.

1. Introduction

The contemporary interest in polyoxovanadates reflects not only their putative electro-, photo-, and mixed ionic properties [1–3], but also the complex structural chemistry of vanadium with a variety of coordination geometries and oxidation states [4]. An important advance in this field is the rational design and preparation of novel organic–inorganic oxovanadium hybrids [5,6]. Incorporation of organic motifs and inorganic vanadium oxides may generate new composite solids. These hybrids are expected to exhibit enhanced properties and functions not seen in pure inorganic or organic phases [7–9]. In studies of those materials, a series of novel oxovanadium hybrids have been isolated, which exhibit interesting one-, two-, and three-dimensional frameworks [6,10,11]. Though many organic–inorganic vanadium oxides are characterized by oxovanadates covalently coordinated to transition metal–ligand complex (TMC), the transition metal in most of these complexes are limited to 3*d* transition metal. The oxovanadium hybrids decorated by 4*d* TMC are rare, especially for V/Ag-complexes. Recent studies have shown that pure inorganic vanadium silver phases, such as $Ag_4V_2O_6F_2$, $Ag_2V_4O_{11}$, $Ag_4V_2O_7$, and α-Ag_3VO_4, exhibit interesting electrochemically active cathode materials [12–15]. However, to our knowledge, only two examples of V–Ag polymers and three examples of the V/Ag/organonitrogen system have been reported [16–18].

Zubieta et al. have reviewed the significant role of organonitrogen component on the structure of the oxovanadium hybrid materials [19]. Judicious selection of organic ligand is very important because deliberately structural changes about organic building blocks such as length, flexibility, and symmetry can dramatically change the final structural motifs of these inorganic–organic hybrids. Recent studies on the supramolecular chemistry of entangled frameworks suggested that the linear flexible *N*, *N*′-bridging ligand, such as the derivatives of imidazole and 1, 2, 4-triazole, may favor unprecedented entangled architectures [20–23]. In this paper, we chose 1,4-bis(triazol-1-ylmethyl)benzene and 1,1′-(1,4-butanediyl)bis(imidazole) as the organonitrogen components for synthesizing the novel silver vanadium composite phases.

We are currently performing investigations on the chemistry of the Ag(I)–organonitrogen–polyoxovanadates family, in order to obtain information at the basic structural level for electro-property study. Herein, we report the successful synthesis and characterization of two new organic–inorganic hybrids, namely, $[Ag(btx)]_4H_2V_{10}O_{28}\cdot 2H_2O$ **1** and $[Ag(biim)]_2V_4O_{11}$ **2**. The two compounds exhibit very rare 2D and 3D poly(pseudo-rotaxane) architectures.

2. Experimental

2.1. General procedures

All chemicals were commercially purchased and used without further purification. Elemental analyses (C, H and N) were performed on a Perkin-Elmer 2400 CHN Elemental Analyzer. IR

* Corresponding authors. Fax: +86 431 5098787.
E-mail addresses: Wangeb889@nenu.edu.cn (E. Wang), Li_juan@jlu.edu.cn (J. Li).

0022-4596/$ - see front matter © 2009 Elsevier Inc. All rights reserved.
doi:10.1016/j.jssc.2009.07.022

spectra were recorded in the range 400–4000 cm^{-1} on an Alpha Centaurt FT/IR Spectrophotometer using KBr pellets. TG analyses were performed on a Perkin-Elmer TGA7 instrument in flowing N_2 with a heating rate of 10 °C min^{-1}. A CHI 660 Electrochemical Workstation connected to a Digital-586 personal computer was used for control of the electrochemical measurements and for data collection. A conventional three-electrode system was used. The working electrodes were compounds **1** and **2** bulk-modified carbon paste electrodes, respectively. A SCE was used as reference electrode and Pt gauze as a counter electrode. The working electrodes were prepared following our earlier method [24].

2.2. Synthesis of $Ag_4(btx)_4H_2V_{10}O_{28}\cdot 2H_2O$ **1**

A mixture of $NaVO_3$ (0.3 mmol), $AgNO_3$ (0.1 mmol), btx (0.1 mmol), four drops of Et_3N/CH_3CN mixture (1:9), CH_3CN (1 mL), and H_2O (9 mL) was placed in a Parr Teflon-lined stainless steel vessel (15 mL), and then the vessel was sealed and heated at 120 °C for three days. After the mixture was slowly cooled to room temperature, red crystals of **1** were obtained (yield: 53% based on V). The initial and final pH of the solutions are 5.42 and 6.88, respectively. Anal. Calcd. for $C_{48}H_{62}Ag_4N_{24}O_{30}V_{10}$: C, 24.06; H, 2.61; N, 14.03%. Found: C, 24.11; H, 2.65; N, 14.09%. IR spectrum (cm^{-1}): 3426(m), 3090(vs), 2926(m), 2854(w), 1641(w), 1516(s), 1425(vs), 1341(vs), 1277(vs), 1206(m), 1131(s), 1101(vm), 945(s), 818(s), 751(w), 724(vs), 674(vs), 639(vs), 588(m), 543(m), 512(w), 457(w).

2.3. Synthesis of $[Ag(biim)]_2V_4O_{11}$ **2**

A mixture of NH_4VO_3 (0.3 mmol), $AgNO_3$ (0.1 mmol), biim (0.1 mmol), four drops of Et_3N/CH_3CN mixture (1: 9), CH_3CN (3 mL), and H_2O (2 mL) was placed in a Parr Teflon-lined stainless steel vessel (15 mL), and then the vessel was sealed and heated at 120 °C for three days. After the mixture was slowly cooled to room temperature, pale-yellow crystals of **2** were obtained (yield: 61% based on V). The initial and final pH of the solutions are 5.67 and 7.01, respectively. Anal. Calcd. for $C_{20}H_{28}Ag_2N_8O_{11}V_4$: C, 24.61; H, 2.89; N, 11.48; V, 20.88; Ag, 22.10%. Found: C, 24.67; H, 2.95; N, 11.43; V, 20.84; Ag, 22.06%. IR spectrum (cm^{-1}): 3154(w), 3116(vs), 2992(m), 2876(w), 2856(w), 1515(s), 1446(s), 1401(m), 1360(m), 1343(vs), 1314(w), 1281(vs), 1250(s), 1223(vs), 1177(w), 1156(m), 1115(s), 1095(vs), 1082(vs), 1039(w), 1027(w), 977(vs), 969(vs), 953(vs), 939(s), 886(vs), 834(s), 783(vs), 768(vs), 673(s), 657(s), 472(s).

2.4. X-ray crystallography

The measurements for compounds **1** and **2** were performed on a Rigaku R-AXIS RAPID IP diffractometer. Compounds **1** and **2** were collected at 293 K, and graphite-monochromated Mo$K\alpha$ radiation ($\lambda = 0.71073$ Å) was used. Empirical absorption corrections were applied for compounds **1** and **2**. The structures were solved by the direct method and refined by the full-matrix least squares on F^2 using the SHELXL-97 software [25,26]. In each structure, hydrogen atoms of organic ligands were fixed in ideal positions. The hydrogen atoms attached to water were not located. All of the non-hydrogen atoms were refined anisotropically.

A summary of crystal data and structure refinements for compounds **1** and **2** is provided in Table 1. Selected bond lengths and angles are listed in Table 2. CCDC 669342 and 669343 contain the supplementary crystallographic data for this paper.

3. Results and discussion

3.1. Synthesis consideration

Hydrothermal reaction has been proved to be an effective technique for preparation of numerous of solid-state oxides and organic–inorganic hybrid materials. Especially, hydrothermal conditions are in favor of capturing structurally more complicated

Table 1
Crystal data and structure refinements for **1** and **2**.

	1	**2**
Formula	$C_{48}H_{62}Ag_4N_{24}O_{30}V_{10}$	$C_{20}H_{28}Ag_2N_8O_{11}V_4$
fw	2396.10	976.00
T (K)	293(2)	293(2)
Crystal system	Triclinic	Monoclinic
Space group	*P*−1	*C2/c*
a (Å)	12.054(2)	13.022(3)
b (Å)	12.336(3)	18.755(4)
c (Å)	13.824(3)	13.403(3)
α (deg)	110.34(3)	90
β (deg)	111.86(3)	107.72(3)
γ (deg)	97.83(3)	90
V (Å^3)	1703.6(6)	3118.1(1)
Z	1	4
ρ_{calcd} (g cm^{-3})	2.336	2.147
μ (mm^{-1})	2.529	2.456
R_{int}	0.1925	0.0473
Data/parameters	5670/ 532	3571/204
Goodness-of-fit on F^2	1.023	1.059
R_1[a] ($I>2\sigma(I)$)	0.0996	0.0458
wR_2[b] ($I>2\sigma(I)$)	0.1350	0.1143
Largest residuals (e Å^{-3})	0.885/−0.789	1.041/−1.289

[a] $R_1 = \sum||F_o|-|F_c||/\sum|F_o|$.
[b] $wR_2 = \sum[w(F_o^2-F_c^2)^2]/\sum[w(F_o^2)^2]^{1/2}$.

Table 2
Select important bond lengths (Å).

Compound **1**			
V(1)–O(4)	1.560(11)	V(2)–O(6)	1.586(10)
V(1)–O(9)	1.760(10)	V(2)–O(8)	1.805(12)
V(1)–O(8)#1	1.822(11)	V(2)–O(11)#1	1.841(10)
V(1)–O(2)	1.953(11)	V(2)–O(3)	1.919(11)
V(1)–O(10)#1	1.968(11)	V(2)–O(5)	2.011(11)
V(1)–O(12)	2.284(10)	V(2)–O(12)#1	2.243(12)
V(3)–O(1)	1.623(11)	V(4)–O(5)	1.646(10)
V(3)–O(11)	1.800(9)	V(4)–O(2)	1.691(10)
V(3)–O(9)	1.833(11)	V(4)–O(13)	1.876(10)
V(3)–O(7)	1.948(11)	V(4)–O(7)	1.953(11)
V(3)–O(13)#1	1.973(10)	V(4)–O(12)	2.079(12)
V(3)–O(12)	2.265(11)	V(4)–O(12)#1	2.118(10)
V(5)–O(14)	1.577(10)	V(5)–O(7)	1.944(10)
V(5)–O(3)	1.758(11)	V(5)–O(13)#1	1.976(10)
V(5)–O(10)	1.898(10)	V(5)–O(12)#1	2.215(11)
Ag(1)–N(1)	2.147(14)	Ag(2)–N(10)	2.054(14)
Ag(1)–N(4)	2.176(13)	Ag(2)–N(7)	2.115(15)
Ag(1)–Ag(1)#2	3.183(3)		
Compound **2**			
V(1)–O(2)	1.604(5)	V(2)–O(6)	1.573(6)
V(1)–O(3)	1.808(5)	V(2)–O(5)	1.720(4)
V(1)–O(5)#2	1.842(4)	V(2)–O(3)	1.748(6)
V(1)–O(1)	1.613(5)	V(2)–O(4)	1.7761(14)
Ag(1)–N(3)	2.101(5)	Ag(1)–N(1)	2.108(5)
Ag(1)–Ag(1)#1	3.2809(12)		

Symmetry transformations used to generate equivalent atoms: for **1**: #1 $-x$, $-y$, $-z$; #2 $-x$+1, $-y$, $-z$; #3 x−1, y, z−1; #4 x+1, y, z+1; #5 x, y, z−1; #6 x, y, z+1; for **2**: #1 $-x$+1,$-y$+1,$-z$; #2 $-x$+1/2, $-y$+1/2, $-z$; #3 $-x$+1, y, $-z$+1/2; #4 $-x$+2, y, $-z$+1/2; #5 $-x$+1/2, $-y$+3/2, $-z$.

metastable phases, intermediate phases and special species. In addition, the aqueous chemistry of vanadium compound is very complex, it is anticipated that vanadate could form different building units under different pH range [2,27]. In our case, a new morphology oxovanadate $[V_4O_{11}]^{2-}$ is obtained at pH 7.01. If the vanadate solution is acidified to about pH 5.42, it undergoes complex hydrolysis polymerization to yield orange decavanadate ions $[H_2V_{10}O_{28}]^{4-}$. This special structure flexibility is of great benefit to construct different extended frameworks.

Because the solubility of silver-imidazolate or -triazole coordination polymer is very low, it is difficult to isolate {Ag_xL_y/polyoxovanadate} phases. The white precipitation of the intermediate Ag-ligand species was found in the products of **1** and **2**. In our and other previous studies, the silver complexes with molybdates can be prepared from the aqueous solvent [28,29]. However, aqueous synthesis for silver complexes with vanadates is rather difficult. Therefore, we utilize the mixed solvent H_2O/MeCN for the crystallization of Ag(I)–organonitrogen–polyoxovanadates. It is found that the mixed solvent in the reaction can reduce the precipitation of the metal hydroxides and further hydrolysis of $[VO_3]^-$ species, increase the solubilities of some intermediate Ag-ligand species, and further form more structurally interesting helix phases. When the ratio of H_2O/MeCN was changed from 9:1 to 2:3, the white precipitation appearing in product **2** was significantly reduced, less than that in product **1**. The interesting eight-shaped helix $\{Ag(biim)\}^+$ and metastable chainlike $[V_4O_{11}]^{2-}$ chains also result in the structure of **2**. This mixed solvent effect could be found more obviously in the structures of **1** without helix motif, although the long flexible btx ligand is induced. In fact, the reaction of $[VO_3]^-$ with silver cationic species in organic solvents is sensitive to slight changes in the experimental conditions. It is very difficult to elucidate the mechanistic details on the formation of these species.

3.2. Structure description

As shown in Fig. 1, the structure of $Ag_4(btx)_4H_2V_{10}O_{28}\cdot 2H_2O$ **1** is constructed from two 1D polymeric chains, $\{Ag_2(btx)_2\}^{2+}$ and $[Ag_2(btx)_2H_2V_{10}O_{28}]^{2-}$, which are assembled by supramolecular forces into an intriguing 2D poly(pseudo-rotaxane) network. The $[V_{10}O_{28}]^{6-}$ cluster, which is built up from ten VO_6 edge- and corner-shared octahedral, is a typical decavanadate (Fig. S2). According to the results of the bond valance sum for all oxygen atoms in $[V_{10}O_{28}]^{6-}$ anion, the two separate protons for the balancing charge should be attached to the two μ_2 bridge oxygen atoms (O10, BVS = 1.414) of $[V_{10}O_{28}]^{6-}$. The V–O (terminal) and the V–O (bridge) bond lengths are in the range of

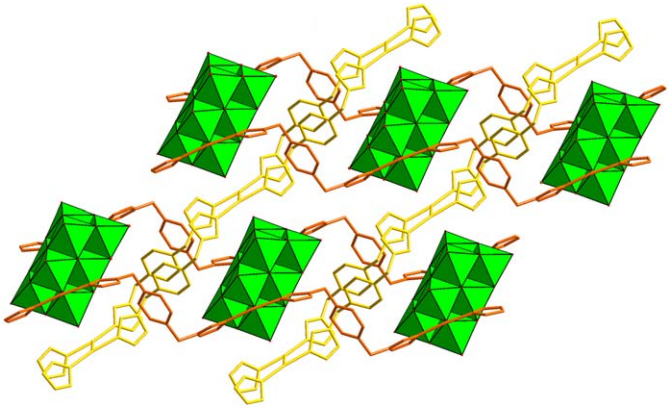

Fig. 1. Ball–stick and polyhedral representation of the 2D polythreaded structure in **1**.

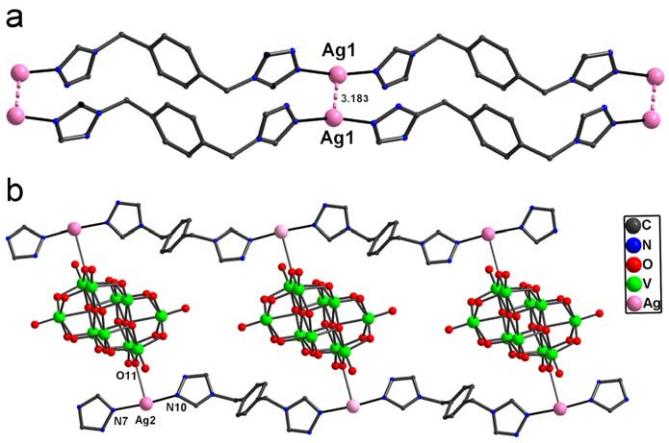

Fig. 2. Ball–stick representation of two kinds of chains of **1**: (a) $\{Ag_2(btx)_2\}^{2+}$ double chain; (b) $[Ag_2(btx)_2H_2V_{10}O_{28}]^{2-}$ ladder like double-chain.

1.606(2)–1.624(2) Å and 1.692(2)–2.284(2) Å, respectively. The V–O–V bond angles vary between 74.97(8)° and 175.78(1)°. All these bond lengths and bond angles are within the normal ranges and in close agreement with those found in previously reported structures of decavanadate salts [30]. The Ag1 atom adopts to linear coordination geometry which is completed by two nitrogen atoms from different btx ligands (Ag1–N1 2.147(1) Å, Ag1–N4 2.176(1) Å). Two {Ag1btx} single chains are held together to form a double chain by argentophilic Ag···Ag interactions with the short silver–silver contacts of 3.183(3) Å, which are shorter than the sum of the van der Waals radii of two silver atoms (3.440(0) Å) (shown in Fig. 2(a)). The three coordinate geometry at the Ag2 atom is defined by two nitrogen donors of the btx ligands (Ag2–N10 2.041(2) Å, Ag2–N7 2.092(8) Å) and one bridging oxygen from the $[H_2V_{10}O_{28}]^{4-}$ anion (Ag2–O 2.648(1) Å). Each isolated $[H_2V_{10}O_{28}]^{4-}$ polyanion provides two μ_2-O atoms to link two Ag ions. Based on the connection mode, the $[H_2V_{10}O_{28}]^{4-}$ connects two adjacent Ag2-btx single chains to generate a ladder like double-chain along the crystallographic *c* axis, as shown in Fig. 2(b). The grids in the ladder is 13.824 × 11.804 Å. Furthermore, each $\{Ag(1)_2(btx)_2\}^{2+}$ double chain penetrates the ladder in an inclined way to form the poly(pseudo-rotaxane) architecture. The Ag1 atoms on the double-chain have weak interactions with the two oxygen atoms from $[H_2V_{10}O_{28}]^{4-}$ (Ag1–O14 2.739(5), Ag1–O6 2.745(9)), which further stabilizes the whole entangled 2D supramolecular sheet. These 2D sheets are further held together to generate a 3D supramolecular structure through hydrogen bonds (OW1···C1 3.052 Å, OW1···C23 2.917 Å, OW1···N7 2.995 Å, OW2···O4 2.974 Å, OW2···C23 2.818 Å) shown in Fig. S3.

The 3D framework of $[Ag(biim)]_2V_4O_{11}$ **2** is composed of the 1D chainlike polyoxoanion $[V_4O_{11}]^{2-}$ entrained within the 3D framework of the $\{Ag(biim)\}_n^{n+}$ coordination polymer, as shown in Fig. 3(a). The vanadate chain $[V_4O_{11}]^{2-}$, shown in Fig. 3(b), is a new type of structural motif, which contains two crystallographically distinct tetrahedrally coordinated vanadium atoms. These vanadium tetrahedral share corners with each other through oxygen atoms, forming infinite $[V_4O_{11}]^{2-}$ chains with the V–O bond lengths in the range of 1.573(6)–1.842(4) Å and O–V–O angles 106.7(3)–111.2(2)°. The vanadate chains may be described as the adjacent $[V_4O_{12}]^{4-}$ clusters which are joined together through sharing a single oxygen atom. This oxygen atom occupies a special position (site occupancy = 0.5). The $[V_4O_{12}]^{4-}$ cluster is a discrete building block in the polyoxovanadate species. It is speculated that there is structural preassembly of the tetravanadate units followed by fusion into the chain structure.

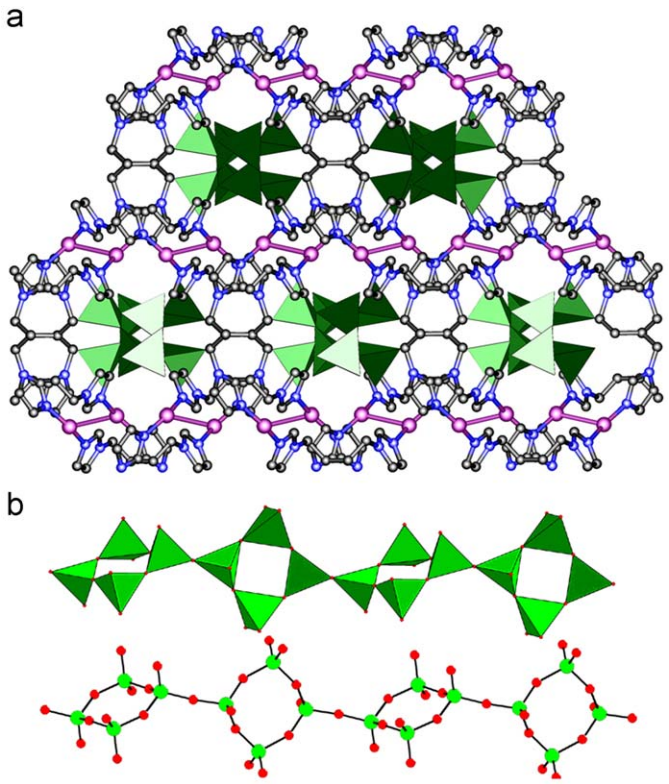

Fig. 3. Ball–stick and polyhedral representation of 3D framework structure (a) and the vanadadate chain $[V_4O_{11}]^{2-}$ (b) of **2**.

To our knowledge, it is the first time this structural unit has been described so far.

There is one crystallization independent silver site in the cationic framework. The three coordinate geometry at the silver is defined by two nitrogen donors of the biim molecules (Ag1–N1 2.108(5) Å, Ag1–N3 2.101(5) Å) and one terminal oxygen atom from the $\{VO_4\}$ tetrahedron (Ag1–O1 2.620(6) Å). The distance of Ag1–O1 is shorter than the sum of the van der Waals radii of Ag and O (3.20 Å), implies weak binding and leads to the T-shaped coordination geometry around Ag1. As shown in Fig. 4, each biim ligand is twisted into a spiral conformation to link two Ag ions, furnishing an unchiral meso-helical $\{Ag(biim)\}_n^{n+}$. The Ag1⋯Ag1 distance is 3.281(1) Å, which is shorter than the sum of the van der Waals radii of two silver atoms (3.440(0) Å), suggesting significant silver (I)–silver (I) interactions. By the aid of the silver(I)–silver(I) interactions, the $\{Ag(biim)\}_n^{n+}$ meso-helixes are linked into a 3D honeycomb framework with *ths* topology, as shown in Fig. 5. The channels in the honeycomb framework possess approximate dimensions of 11.466 × 13.022 Å. And then, each 1D inorganic vanadate chain penetrated the channel by the weak interactions between terminal oxygen atom and Ag sites, as shown in Fig. 5.

The structure can be alternatively viewed as the adjacent $[V_4O_{11}]^{2-}$ chains linked up through the $\{Ag(biim)\}_n^{n+}$ chains to form a 3D framework with large porous in three dimensions, as shown in Fig. S4. The big sizes of the channel in the two individual frameworks allow an interesting two-fold interpenetrated to occur. The silver (I)–silver (I) interactions stabilize the whole entanglement.

In the structures presented here, the versatility of secondary metal complexes (SMCs) play very important roles for directing the architecture of the vanadium anion component. It is clear that the SMCs $\{Ag(btx)\}^+$ in **1** is observed to be charge-balancing cation and bridging groups. The $\{Ag(biim)\}^+$ in **2** acts as a template for

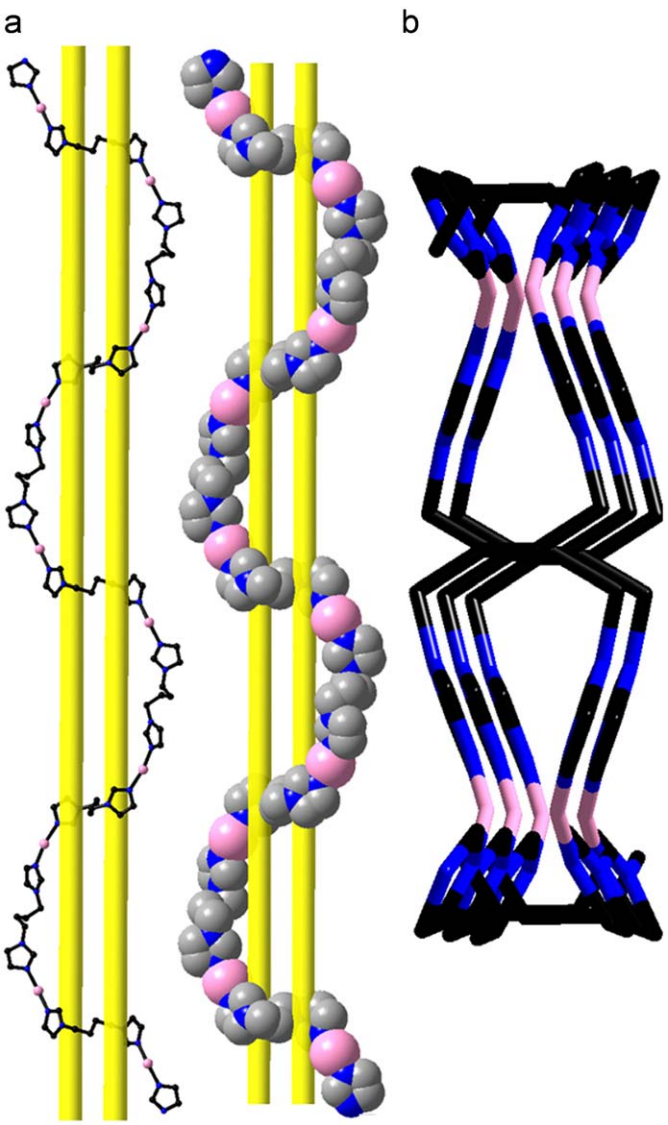

Fig. 4. (a) Ball–stick and space–filling and (b) stick views of the meso-helix of $\{Ag(biim)\}^+$ in **2**.

the formation of the new $[V_4O_{11}]^{2-}$ chain. Compound **2** can also be viewed as a successful case by employing a 'ship in the bottle' approach. Similar strategy has ever been used in molybdenum oxides, such as the 3D complexes, $[\{Fe(tpypor)\}_3Fe(Mo_6O_{19})_2]\cdot x$-$H_2O$ [31], $[\{Cu_2(triazolate)_2(H_2O)_2\}Mo_4O_{13}]$ [32] and $[Cu^{I}_3Cl(4,4'$-$bipy)_4][Cu^{II}(phen)_2Mo_8O_{26}]$ [33]. To our knowledge, no such compound based on polyoxovanadates is reported.

3.3. FT-IR spectroscopy

In the IR spectrum of compound **1**, the characteristic peaks at 945, 818, 751, 724, 674, 639, 588, 543, 512, 457 cm^{-1} are attributed to the $\nu(V=O)$, $\nu(V–O–M)$ (M = V or Ag) vibrations. Comparing the IR spectrum of compound **1** with that of $[V_{10}O_{28}]^{6-}$ polyoxoanion [29], it can be observed that the shape of peaks in the range 600–1000 cm^{-1} is nearly identical to that of $[V_{10}O_{28}]^{6-}$ except slight shifts of some peaks due to the effect of coordination, which indicates that the polyoxoanion in compound **1** still retains the basic $[V_{10}O_{28}]^{6-}$ structure. This is in agreement with the result of single-crystal X-ray diffraction analysis. In addition, the characteristic bands at 3090, 2926, 1516, 1425, 1341, 1277, 1206,

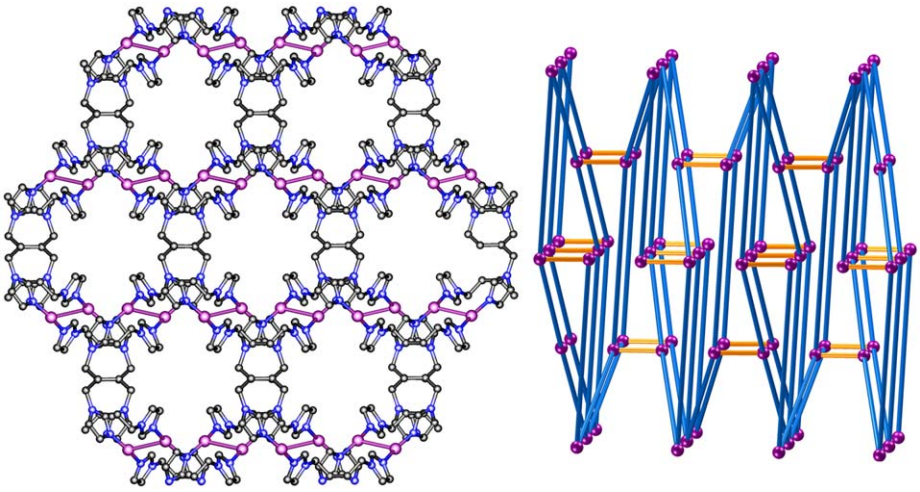

Fig. 5. Ball and stick (left) and the schematic diagram (right) of the honeycomb pattern of the $\{Ag(biim)\}_n^{n+}$ framework through the Ag···Ag contacts (orange bars). [For interpretation of the references to color in this figure legend, the reader is referred to the webversion of this article.]

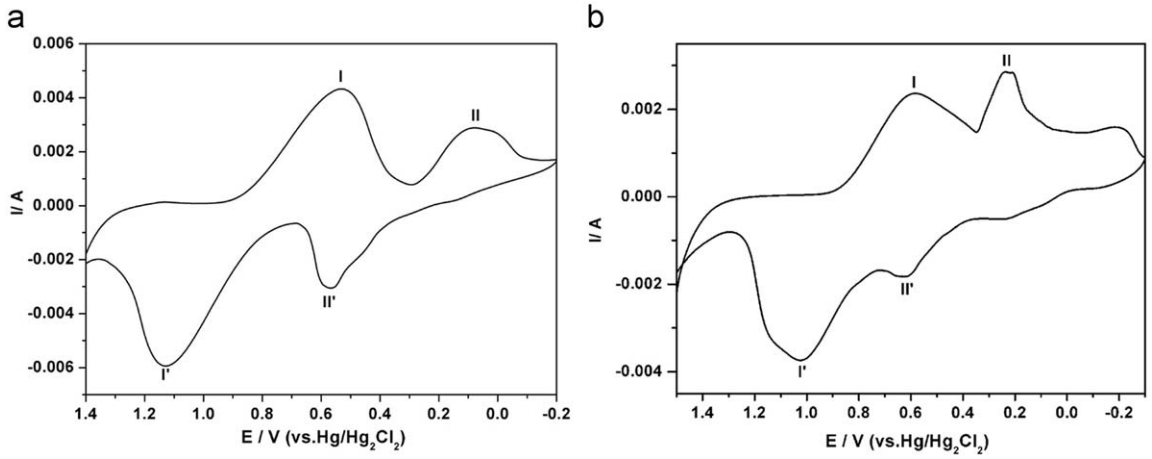

Fig. 6. The cyclic voltammograms in 1 M H_2SO_4 at 5 mV s^{-1} scan rate for **1** (a) and **2** (b).

1131, and 1101 cm^{-1} can be regarded as features of the btx molecules. The broad peak at 3430 cm^{-1} and the strong peak at 1640 cm^{-1} are attributed to the lattice water molecules in **1**.

In the IR spectrum of compound **2**, the characteristic peaks at 977, 969, 953, 939, 886, 834, 783, 768, 673, 657, and 472 cm^{-1} are attributed to the $\nu(V=O)$, $\nu(V–O–M)$ (M = V or Ag) vibrations. Additionally, the characteristic bands at 3116, 2992, 1515, 1446, 1401, 1360, 1343, 1281, 1250, 1223, 1156,1115, 1095, and 1082 cm^{-1} can be regarded as features of the biim molecules (Supporting Information Figs. S5 and S6).

3.4. Thermogravimetric analyses

The thermogravimetric analyses were carried out in flowing N_2 with a heating rate of 10 °C min^{-1} in the temperature range 25–600 °C for compounds **1** and **2**, as shown in Fig. S7 and S8. The TG curve of compound **1**, the weight loss occurs in the 25–250 °C temperature range (ca. 0.91%) corresponding to the release of water molecules per formula unit. The weight losses (ca. 38.93%) from 279 to 440 °C can be attributed to the decomposition of btx ligands. The observed weight loss (39.84%) is consistent with the calculated value (41.90%). The sample does not lose weight at temperatures higher than 440 °C. In the curve of compound **2**, five continuous weight losses in the range of 210–520 °C corresponds to the loss of biim ligands. The whole weight loss 37.99% is in agreement with the calculated value 38.93%. The sample does not lose weight at temperatures higher than 520 °C. Considering the nitrogen protected environment of the TG analyses procedure, we speculate both compounds decomposed into simple metal oxide.

3.5. Electrochemical property

POMs have attracted much interest in electrode modification and electrocatalysis fields because of their ability to undergo a series of reversible multielectron redox processes. Especially, vanadium oxides are of particular interest as candidates for active cathode materials in reversible lithium batteries or electrochemical devices. Silver vanadium oxide has well characterized through the years and is the major commercially used cathode in lithium batteries. While various silver vanadium oxides are known, the V/Ag/organonitrogen system and their properties are rarely explored. To determine the redox properties of compounds **1** and **2**, compounds-bulk-modified carbon paste electrode (CPE) was fabricated as the working electrode due to their insolubility in most solvents [34]. Chemically bulk-modified CPE is a mixture of a modifier, graphite powder and pasting liquid, which has been widely applied in electrochemistry owing to its many advantages: inexpensive, easy to handle and prepare. The bare graphite

electrode did not show redox property. Therefore, the peaks found in the figures reflect the properties of the compounds.

Fig. 6(a) and (b), respectively, shows the voltammetric behavior of the working electrodes at 5 mV s^{-1} scan rate for **1** and **2** in the 1 M H_2SO_4 aqueous solution. The compounds **1** and **2** exhibit two quasi-reversible redox peaks appear. The redox peaks I–I′ in the potential range may correspond to V(V)/V(IV) one-electron processes except some displacements, and the mean peak potentials $E_{1/2} = (E_{pa}+E_{pc})/2$ of the quasi-reversible redox peaks I–I′ are 0.832V in **1** and 0.807 V in **2** respectively. The mean peak potentials of II–II′ are 0.327 V in **1** and 0.427 in **2**, respectively, and the waves II–II′ can be ascribed to the redox of Ag(I). The peak-to-peak separations between the corresponding anodic and cathodic peaks (ΔE_p) at the working electrode are larger than the reversible surface redox process, which might be due to non-ideal behavior.

Fig. S9 shows the cyclic voltammograms of the at different scan rates of **1**-CPE and **2**-CPE in the 1 M H_2SO_4 aqueous solution. When the scan rate was changed from low to high, the peak potentials in both compounds changed gradually: the cathodic peak potentials shifted to the negative direction and the corresponding anodic peak potentials shifted to the positive direction with increasing scan rate. It should be pointed out that the peak-to-peak separation between the corresponding cathodic and anodic peaks in compounds-CPE increases along with the scan rate.

4. Conclusion

In summary, we have successfully synthesized two new hybrids based on polyoxovanadates, $[H_2V_{10}O_{28}]^{4-}$ and $[V_4O_{11}]^{2-}$, and Ag–organonitrogen polymers. Compounds **1** and **2** are self-assembled to form the poly(pseudo-rotaxane) architectures, and represent two new examples of polyoxovanadates–Ag–organonitrogen family. Extended research on the structural chemistry of this system may focus on the replacement of oxovanadates and ligands. Studies in this respect are underway to reveal the synthetic rules and to explore their attractive properties.

Acknowledgment

This work was financially supported by the National Science Foundation of China (20371011).

Appendix A. Supplementary material

Supplementary data associated with this article can be found in the online version at doi:10.1016/j.jssc.2009.07.022.

References

[1] L.C.W. Baker, D.C. Glick, Chem. Rev. 98 (1998) 3–50.
[2] T. Chirayil, P.Y. Zavalij, M.S. Whittingham, Chem. Mater. 10 (1998) 2629–2640.
[3] F. Garcia-Alvarado, J.M. Tarascon, B. Wilkens, J. Electrochem. Soc. 139 (1992) 3206–3214.
[4] V. Soghomonian, Q. Chen, R.C. Haushalter, J. Zubieta, Angew. Chem. Int. Ed. Engl. 34 (1995) 223–226.
[5] P.J. Hagrman, J. Zubieta, Inorg. Chem. 39 (2000) 3252–3260.
[6] A. Tripathi, T. Hughbanks, A. Clearfield, J. Am. Chem. Soc. 125 (2003) 10528–10529.
[7] M.J. Manos, A.J. Tasiopoulos, E.J. Tolis, N. Lalioti, J.D. Woollins, A.M.Z. Slawin, M.P. Sigalas, T.A. Kabanos, Chem. Eur. J. 9 (2003) 695–703.
[8] K. Hegetschweiler, B. Morgenstern, J. Zubieta, P.J. Hagrman, N. Lima, R. Sessoli, F. Totti, Angew. Chem. 116 (2004) 3518–3521.
[9] L. Chen, F.L. Jiang, Z.Z. Lin, Y.F. Zhou, C.Y. Yue, M.C. Hong, J. Am. Chem. Soc. 127 (2005) 8588–8589.
[10] J. Tao, X.M. Zhang, M.L. Tong, X.M. Chen, J. Chem. Soc. Dalton Trans. (2001) 770–771.
[11] Y.F. Qi, Y.G. Li, C. Qin, E.B. Wang, H. Jin, D.R. Xiao, X.L. Wang, S. Chang, Inorg. Chem. 46 (2007) 3130–3217.
[12] C.C. Liang, M.E. Bolster, R.M. Murphy, US Patent 4,391,729, July 5, 1983.
[13] T.A. Albrecht, C.L. Stern, K.R. Poeppelmeier, Inorg. Chem. 46 (2007) 1704–1708.
[14] E.M. Sorensen, H.K. Izumi, J.T. Vaughey, C.L. Stern, K.R. Poeppelmeier, J. Am. Chem. Soc. 127 (2005) 6347–6352.
[15] M.I. Bertoni, N.J. Kidner, T.O. Mason, T.A. Albrecht, E.M. Sorensen, K.R. Poeppelmeier, J. Electroceram. 18 (2007) 189–195.
[16] B. Zhao, L. Yi, P. Cheng, D.Z. Liao, S.P. Yan, Z.H. Jiang, Inorg. Chem. Commun. 7 (2004) 971–973.
[17] K. Barthelet, D. Riou, G. Férey, Solid State Sci. 3 (2001) 203–209.
[18] H.S. Lin, P.A. Maggard, Inorg. Chem. 47 (2008) 8044–8052.
[19] D.J. Chesnut, D. Hagrman, P.J. Zapf, R.P. Hammond, R. LaDuca, R.C. Haushalter, J. Zubieta, Coord. Chem. Rev. 190–192 (1999) 737–769.
[20] S.L. Li, Y.Q. Lan, J.F. Ma, J. Yang, X.H. Wang, Z.M. Su, Inorg. Chem. 46 (2007) 8283–8290.
[21] X.R. Meng, Y.L. Song, H.W. Hou, H.Y. Han, B. Xiao, Y.T. Fan, Y. Zhu, Inorg. Chem. 43 (2004) 3528–3536.
[22] J.F. Ma, J.F. Liu, Y. Xing, H.Q. Jia, Y.H. Lin, J. Chem. Soc. Dalton Trans. (2000) 2403–2407.
[23] L. Song, J.R. Li, P. Lin, Z.H. Li, T. Li, S.W. Du, X.T. Wu, Inorg. Chem. 45 (2006) 10155–10161.
[24] X.L. Wang, E.B. Wang, Y. Lan, C.W. Hu, Electroanalysis 14 (2002) 1116–1121.
[25] G.M. Sheldrick, SHELXS 97, Program for Crystal Structure Solution, University of Göttingen, Göttingen, Germany, 1997.
[26] G.M. Sheldrick, SHELXL 97, Program for Crystal Structure Refinement, University of Göttingen, Göttingen, Germany, 1997.
[27] T.G. Chirayil, E.A. Boylan, M. Mamak, P.Y. Zavalij, M.S. Whittingham, Chem. Commun. (1997) 33–34.
[28] C. Streb, C. Ritchie, D.L. Long, P. Kögerler, L. Cronin, Angew. Chem. Int. Ed. 46 (2007) 7579–7582.
[29] H.A. Alexandra, L. Pickering, D.L. Long, P. Kögerler, L. Cronin, Chem. Eur. J. 11 (2005) 1071–1078.
[30] H. Kumagai, M. Arishima, S. Kitagawa, K. Ymada, S. Kawata, S. Kaizaki, Inorg. Chem. 41 (2002) 1989–1992.
[31] D. Hagrman, P.J. Hagrman, J. Zubieta, Angew. Chem. Int. Ed. Engl. 38 (1999) 3165–3168.
[32] D. Hagrman, J. Zubieta, Chem. Commun. (1998) 2005–2006.
[33] H. Jin, Y.F. Qi, E.B. Wang, Y.G. Li, C. Qin, X.L. Wang, S. Chang, Eur. J. Inorg. Chem. (2006) 4541–4545.
[34] L.Y. Duan, F.C. Liu, X.L. Wang, E.B. Wang, C. Qin, J. Mol. Struct. 705 (2004) 15–20.